Novel structural features and phase transition behaviour of $(Sr_{1-x}Ca_x)TiO_3$: II. X-ray diffraction studies

1999 J. Phys.: Condens. Matter 11 2247

(http://iopscience.iop.org/0953-8984/11/10/011)

J. Phys.: Condens. Matter **11** (1999) 2247–2258. Printed in the UK PII: S0953-8984(99)95431-0

Novel structural features and phase transition behaviour of $(Sr_{1-x}Ca_x)TiO_3$: II. X-ray diffraction studies

Rajeev Ranjan and Dhananjai Pandey

School of Materials Science and Technology, Institute of Technology, Banaras Hindu University, Varanasi-221005, India

Received 29 June 1998, in final form 9 December 1998

Abstract. Results of a careful XRD study of the room temperature structure of $(Sr_{1-x}Ca_x)TiO_3$ (SCT) with $0.0 \leqslant x \leqslant 1.0$ are presented to show that the structure of SCT is $CaTiO_3$- (CT-) like for $x \geqslant 0.12$. High temperature XRD studies on the phase transition behaviour of SCT with $0.12 \leqslant x \leqslant 0.21$ show the existence of an intermediate phase in between the room temperature orthorhombic phase and the high temperature cubic phase. This is analogous to the phase transition behaviour of pure CT and is attributed to the softening of the R_{25} and M_3 point phonon modes.

1. Introduction

Phase transitions in ABO_3 oxide perovskites (A = Na, K, Ba, Ca, Pb, La, Pr etc, B = Nb, Ta, Ti, Zr, Al etc) and AMF_3 fluoroperovskites (A = K, Rb, Cs, Tl etc, M = Mn, Cd, Mg etc) have received wide attention from scientific [1, 2] as well as technological [3] angles. All these perovskite materials are necessarily cubic above a critical temperature at normal pressures. On lowering the temperature, some of them undergo [2] a variety of structural phase transitions driven by the softening of zone centre phonons (such as $BaTiO_3$, $PbTiO_3$, $KNbO_3$ etc), one or more zone boundary phonons (such as $SrTiO_3$, $KMnF_3$, $LaAlO_3$ etc) or an electron–phonon interaction leading to cooperative Jahn–Teller distortion (such as in $PrAlO_3$). Amongst the transitions driven by the zone boundary phonons, the 105 K antiferrodistortive phase transition in $SrTiO_3$ (ST) is the simplest and by far the most extensively investigated too. The cubic to tetragonal transition around 105 K in this system results [4] from the freezing of one of the triply degenerate R_{25} modes in which the adjacent octahedra vibrate about one of the cubic $\langle 100 \rangle$ axes. The space group of the low temperature tetragonal phase is $I4/mcm$ and it belongs to the $a^0a^0c^-$ tilt system in the Glazers' classification [5, 6], where the '−ve' tilt signifies the 'antiphase' rotation of TiO_6 octahedra in successive layers about the cubic [001] axis. A similar transition occurs in $KMnF_3$ also at 186 K. However, on further cooling, $KMnF_3$ [2] undergoes another structural transition at 91 K arising from the condensation of the M_3 mode in which the adjacent octahedra vibrate in the same sense. In Glazer's classification, the two low temperature phases of $KMnF_3$ would belong to the $a^0a^0c^-$ and $a^0b^+c^-$ tilt systems.

As pointed out in part I, the room temperature structure of CT belongs to the orthorhombic $Pbnm$ space group with $a^-a^-c^+$ tilt system. In analogy with other perovskites, it is expected that the orthorhombic CT would have resulted from a cubic aristotype (space group $Pm3m$ and tilt system $a^0a^0a^0$) phase below a certain temperature. The tilt system of the room temperature phase suggests that it has resulted from the softening of the R_{25} (−ve tilt) as well as M_3 (+ve tilt) modes. However, unlike many other perovskite systems, the phonon modes in CT and

0953-8984/99/102247+12$19.50

their freezing behaviour have not been investigated despite the fact that the name perovskite for this family of compounds was first coined for CT discovered as a mineral. Only recently, have some attempts been made to understand the phase transition behaviour of CT [7, 8].

In the mixed SCT system, one obviously expects a crossover from ST type phase transition behaviour at low calcium concentrations to CT type behaviour for higher calcium concentrations. In part I of this series of papers, we showed that the room temperature structure of SCT is CT-like for $x \geqslant 0.12$ while it is ST-like for $x \leqslant 0.06$. In the present work, we present the results of a careful room temperature XRD study of SCT powders in support of the structural models presented in part I. We also present the results of a first high temperature powder XRD study on SCT12, SCT15, SCT18 and SCT21 which shows that the phase transition behaviour of SCT samples for $x \geqslant 0.12$ is CT-like in the sense that there is an interposed pseudotetragonal structure between the room temperature orthorhombic and the high temperature cubic phase. Our work shows that the transition temperatures in SCT samples for $x \leqslant 0.25$ are less than 573 K which, unlike the extremely high transition temperatures in CT, are easily achievable for future Raman scattering and other related experiments for settling the mechanism of phase transition via the successive softening of the M_3 and the R_{25} point phonons.

2. Experiment

2.1. Room temperature and high temperature XRD

Room temperature XRD studies were carried out using Cu Kα radiation on a 12 kW Rigaku rotating anode powder diffractometer system fitted with a curved crystal graphite monochromator. All the data collection was done at 9 kW. For room temperature XRD, a scan rate of 1° min^{-1} with a step width of 0.01 degree was used for low angle ($2\theta < 70^\circ$) reflections whereas for high angle reflections in the 2θ range 100–130°, a scan rate of 1° min^{-1} with an optimized step width ($\Delta 2\theta$) of 0.006 to 0.008° was used. For the high temperature powder XRD experiments, commercially available high temperature attachment provided by Rigaku was not used since the high angle reflections of our interest ($2\theta > 100^\circ$) are extremely weak in intensity even under normal experimental conditions. On top of this, the Ni filters at the walls of the high temperature camera reduce the overall intensity so drastically that it is almost impossible to resolve the high angle profiles from the background. In fact, even at room temperature it is not possible to resolve the profile splittings for these high angle reflections without using the curved crystal monochromator which brings down the background counts drastically. However, the commercial high temperature camera provided by Rigaku cannot be used in conjunction with the monochromator. A heating assembly capable of going up to 300 °C was therefore designed which could be used in conjunction with the monochromator. A chromel–alumel thermocouple was embedded just below the specimen surface facing the x-ray beam and the temperature was controlled within ± 2 °C. The stability of the temperature over the entire region was confirmed by repeating the experiments with thermocouple tip placed at different locations. The temperature measurement was verified by comparing the transition temperatures for some ferroelectric and antiferroelectric systems as determined by our high temperature XRD setup with those determined from high temperature dielectric measurements.

2.2. Sample preparation

SCT6, SCT12, SCT25 and SCT50 samples prepared by the semi-wet route described in part I were used in the present investigation. In addition, SCT15, SCT18, SCT21, ST and CT were

prepared using the conventional solid state route. For this, powders of $SrCO_3$, $CaCO_3$ and TiO_2 (purity 99.5%) were ball milled in zirconia jar using zirconia balls with acetone as mixing media. Ball milled powders were then calcined at 1100 °C for 6 h. The calcined powders were crushed and ball milled to break the agglomerates. The SCT powders so obtained were then pelletized (∼1 cm diameter) at a load of 60 kN with 2% PVA solution as a binder and sintered at 1300 °C for 6 h. Sintered pellets were crushed and then annealed at 600 °C to remove strains induced by crushing before using them for diffraction studies.

3. Results and discussion

3.1. Room temperature studies

3.1.1. Superlattice reflections. In the orthorhombic CT, the TiO_6 octahedra are tilted in an 'antiphase' manner leading to the doubling of the elementary perovskite cell. This gives rise to a series of superlattice reflections on the diffraction pattern as shown in figure 1. The strongest superlattice reflection in this XRD pattern has 103 orthorhombic indices. This reflection persists in the XRD patterns of SCT50 and SCT25 also. However, the other superlattice reflections shown in figure 1 for CT are not discernible on XRD patterns of SCT samples. The intensity of the 103 reflection normalized with the intensity of the strongest reflection with orthorhombic indices 200 decreases drastically with decreasing Ca content as shown in figure 2. As already shown in part I, many more superlattice reflections become discernible on the powder neutron diffraction patterns for the SCT samples with $x = 0.50$, 0.25 and 0.12. The vanishingly small intensity of the superlattice reflections other than 103 in the XRD patterns is due to the lower scattering factor of oxygen atoms whose displacements from their ideal cubic positions are basically responsible for the superlattice peaks.

3.1.2. Orthorhombic distortion. The presence of the superlattice reflections in the x-ray and neutron powder diffraction patterns confirms that the structure of SCT for $x \geqslant 0.12$ is orthorhombic at room temperature. The orthorhombic cell parameters as determined by the least squares method using the peak positions of 112, 002, 220, 312, 224 and 116/332 orthorhombic reflections are given in table 1. For comparison, we also give the cubic unit cell parameters for SCT6 and ST in the same table. It is evident from the unit cell parameters given in this table that the orthorhombic distortion for SCT is much smaller than that of CT. The main effect of substitution of Sr^{2+} by Ca^{2+} is a monotonic decrease in the unit cell volume as shown in figure 3. In this figure, the unit cell volumes of ST and SCT6 have been multiplied by a factor of 4 for comparison with the orthorhombic unit cell volumes of SCT ($x \geqslant 0.12$) and CT. The decrease in the unit cell volume of SCT with increasing calcium content is very much expected on the basis of the higher ionic radius of Sr^{2+} ($r = 1.12$ Å) as compared to that of Ca^{2+} ($r = 0.99$ Å).

Table 1. Refined cell parameters and cell volume of $Sr_{1-x}Ca_xTiO_3$.

x	a (Å)	b (Å)	c (Å)	V (Å^3)
1.00	5.446(6)	5.389(1)	7.647(2)	224.4(1)
0.50	5.475(1)	5.480(1)	7.752(2)	232.6(2)
0.25	5.500(1)	5.487(1)	7.800(2)	235.4(2)
0.12	5.518(2)	5.521(2)	7.800(2)	237.6(2)
0.06	3.912(1)			59.86(7)
0.00	3.908(1)			59.68(7)

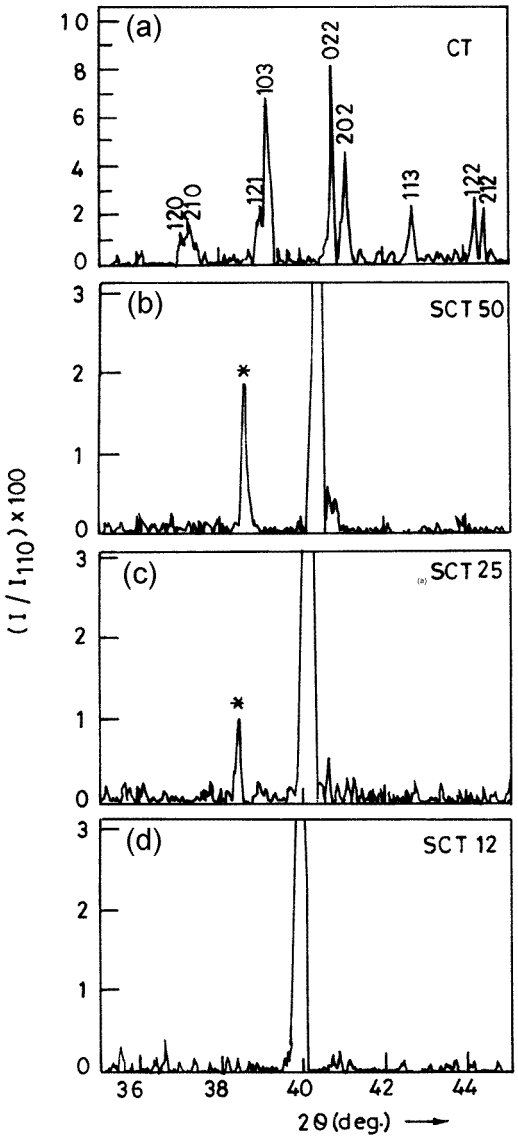

Figure 1. Part of the XRD patterns of $(Sr_{1-x}Ca_x)TiO_3$ for (a) $x = 1.00$, (b) $x = 0.50$, (c) $x = 0.25$ and (d) $x = 0.12$. The 103 superlattice reflection is marked with an asterisk in (b) and (c).

The small orthorhombic distortions listed in table 1 lead to splitting of some of the high angle lines for $x \geqslant 0.12$ except for compositions near $x = 0.50$. For $x = 0.12$ and 0.25, the equivalent elementary perovskite cell parameters (which are related to the orthorhombic cell parameters as $a_o = \sqrt{2}a_p$, $b_o = \sqrt{2}b_p$, $c_o = 2c_p$), a_p and b_p are nearly equal giving rise to pseudo-tetragonal XRD patterns. The c_p is significantly different from $a_p \approx b_p$ for $x = 0.25$ but this difference decreases with decreasing x up to $x = 0.12$. As a result, the splitting of the XRD lines also decreases as x decreases from 0.25 to 0.12. For $x = 0.50$, the a_p, b_p and c_p are nearly equal giving rise to a pseudo-cubic pattern. The only signature of non-cubic symmetry for SCT50 is the extra broadening of the XRD profiles for high angle reflections like

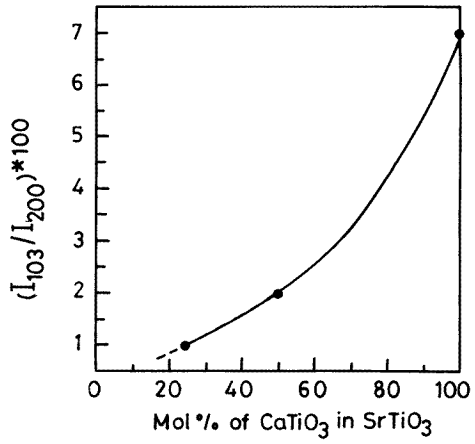

Figure 2. Variation of the peak intensity of the 103 superlattice reflection normalized with respect to the peak intensity of the 200 reflection, with calcium content.

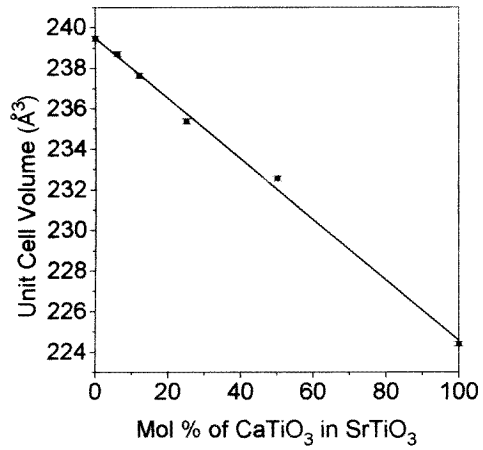

Figure 3. Variation of the room temperature orthorhombic cell volume of $(Sr_{1-x}Ca_x)TiO_3$ with calcium content.

008/440, 028/336/532 and 228/444/620. In fact, only for pure CT does one clearly observe orthorhombic splitting (see e.g. well resolved 022 and 202 reflections in figure 1). For the rest of the compositions, the structure revealed by XRD is either pseudo-tetragonal (SCT12 and SCT25) or pseudocubic (SCT50). We would like to emphasize that but for the knowledge of the positional coordinates of Sr^{2+}/Ca^{2+}, O^{2-} and Ti^{4+} as obtained from Rietveld analysis of the neutron powder diffraction data presented in part I, it would have been impossible to establish the orthorhombic symmetry of SCT with $x \geqslant 0.12$ using XRD data alone. Mitsui and Westphal [9] have assigned tetragonal structure to SCT samples with $0.10 < x < 0.20$ because they used the XRD technique which could not reveal the orthorhombic structure for these compositions. We would like to mention that the unit cell parameters determined using the XRD data are slightly different from those obtained from the neutron powder diffraction data given in part I. In order to decide which of the two sets of parameters represents the correct values, we have simulated the XRD patterns for SCT25 using the DBWS 9411 program [10]

with the positional coordinates and the unit cell parameters given in part I as input parameters. A part of the simulated pattern showing the profiles for the 532, 336 and 028 group of reflections is given in figure 4(a). In the simulated pattern, the 336 and 028 reflections occur on the higher angle side of the 532 reflection whereas in the experimentally observed profiles shown in figure 4(b) the situation is reversed. Further, the observed peak position of the strongest reflection in this triplet (i.e. 532) is also not correctly reproduced in the simulated pattern. Notwithstanding the difference in the peak positions of the three reflections in the simulated and the observed patterns, the relative intensities are in reasonable agreement. This clearly indicates that the positional coordinates given in part I are definitely reliable but not the cell constants presumably due to the poor resolution of the neutron spectrometer ($\Delta d/d \sim 1\%$) as compared to our the x-ray powder diffractometer. Use of the unit cell parameters obtained from the XRD data in conjunction with the positional coordinates obtained by the Rietveld analysis in part I for simulating the XRD patterns not only reproduces the observed relative intensities correctly but also the peak positions as shown in figure 4(b). From this we conclude that the cell parameters given in this paper are more reliable than those given in part I.

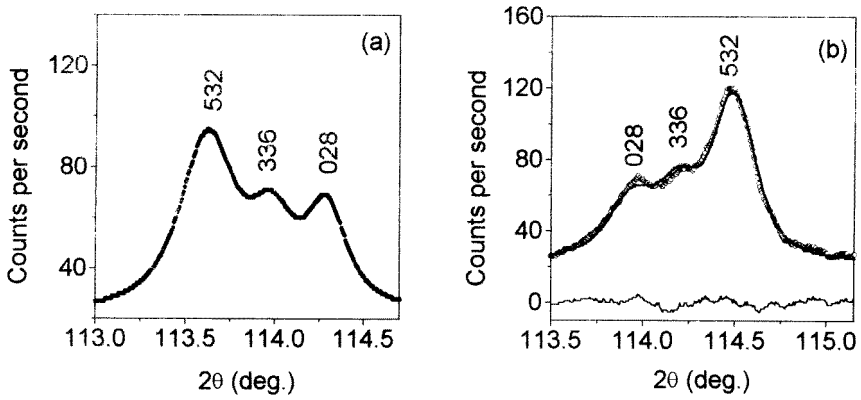

Figure 4. (a) A part of the simulated XRD profile for SCT25, showing the profiles for 532, 336 and 028 set of reflections, obtained using the refined structural parameters given in part I. (b) Observed (· · ·), simulated (——) and difference XRD profile for 532, 336 and 028 set of reflections as obtained using the positional coordinates given in part I in conjunction with the x-ray cell parameters.

3.2. High temperature phase transition studies

The results presented in the previous sections and part I of this series clearly suggest that the structure of SCT for $x \geqslant 0.12$ is CT-like. In this section we shall present experimental evidence to show that the sequence of high temperature structural phase transitions in SCT is also similar to what is known [7] for pure CT. Redfern [7] has recently carried out a detailed study of high temperature structural phase transitions in CT using the powder XRD technique. In his investigations, he has concentrated on the 020/202 pair of well resolved reflections as well as the {121, 103, 211} triplet and {120, 210} doublet of superlattice reflections. As pointed out in the preceding section, 022 and 202 are not resolved in SCT samples because the a_p and the b_p parameters are nearly equal. Further, out of the two set of reflections, the {121, 103, 211} triplet is not discernible for SCT with $x < 0.25$ as shown in figure 1, whereas the intensity of the {120, 210} doublet is too small to be observable on XRD patterns for all the SCT compositions investigated by us. In our high temperature XRD studies, we have concentrated on the 220, 116, 512, 440, 532 and 228 group of reflections for which the data

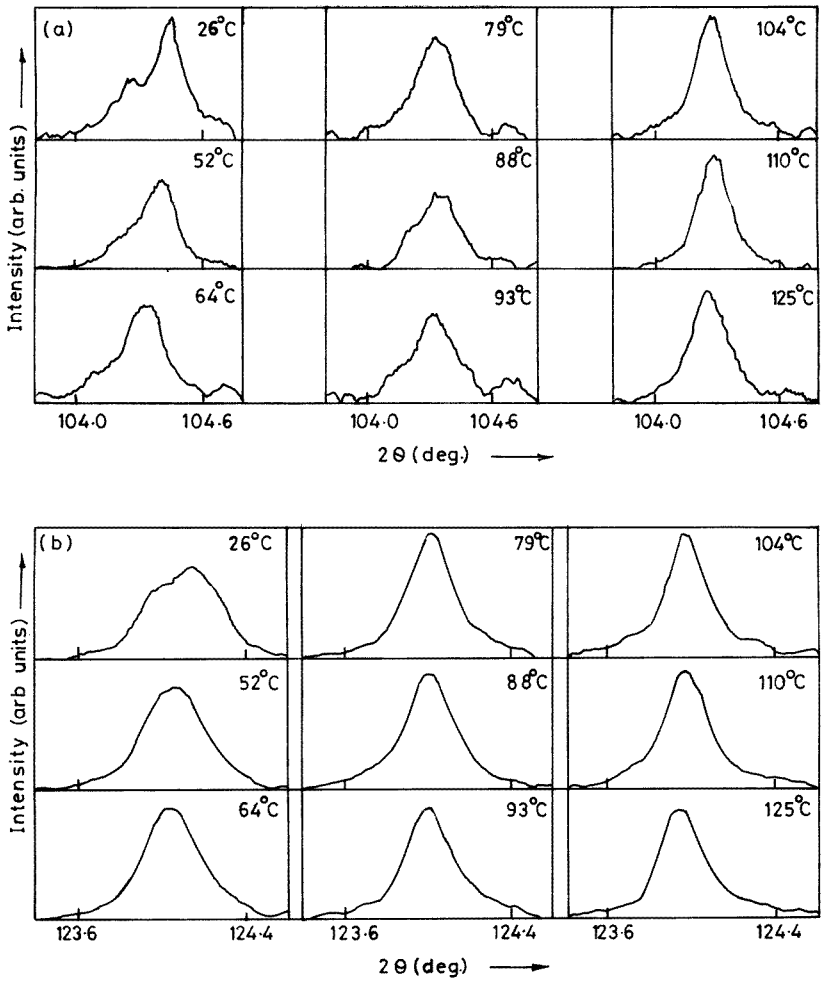

Figure 5. Temperature dependence of the XRD profiles for (a) 008 and 440 and (b) 444, 620, 228 set of reflections for SCT12.

were collected as a function of temperature for SCT12, SCT15, SCT18 and SCT21. Figure 5 depicts the temperature evolution of the XRD profiles of the {008, 440} and {228, 444, 620} group of reflections for SCT12 by way of illustration.

It is evident from this figure that with increasing temperature, the two well resolved profiles at room temperature gradually approach each other and then become singlets. The widths of these apparently singlet profiles, however, continue to decrease with temperature suggesting the presence of overlapping profiles due to noncubic structure. It is possible to determine the transition temperatures from the temperature variation of the full width at half maximum (FWHM) of the {228, 444, 620} set of reflections. For the {008, 440} set of reflections, FWHM analysis could not be of much help since the intensity of the 008 reflection is slightly lower than half the intensity of the 440 reflection. For this set of reflections, we therefore used the full width at quarter maximum (FWQM). Figures 6, 7, 8 and 9 depict the variation of the FWHM/FWQM of the two sets of reflections for SCT12, SCT15, SCT18 and SCT21 respectively. It is evident from these figures that both FWHM (for 228, 444, 620) and FWQM

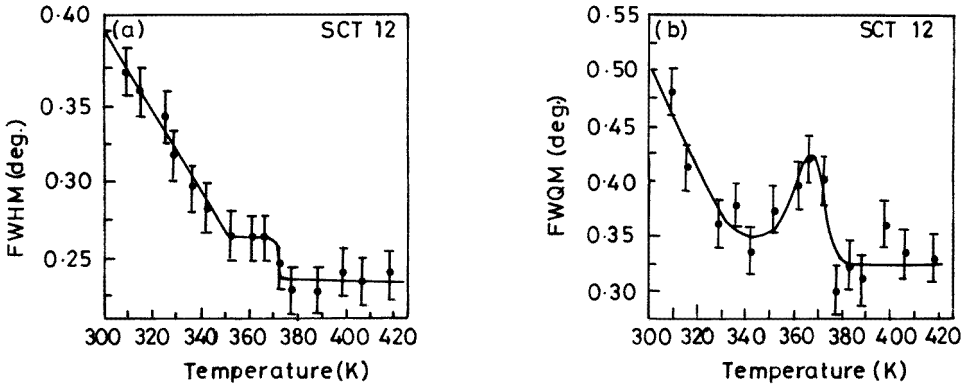

Figure 6. Temperature variation of (a) full width at half maximum (FWHM) of 228, 444, 620 triplet of reflections and (b) full width at quarter maximum (FWQM) of 008, 440 doublet for SCT12.

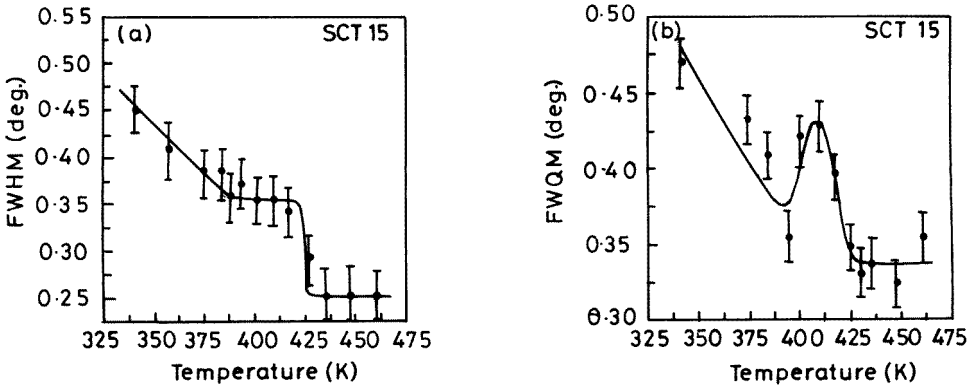

Figure 7. Temperature variation of (a) full width at half maximum (FWHM) 228, 444, 620 triplet of reflections and (b) full width at quarter maximum (FWQM) of 008, 440 doublet for SCT15.

(for 008, 440) decrease up to a temperature $T_1 = 348$, 398, 426 and 480 K for SCT12, SCT15, SCT18 and SCT21 respectively. Beyond this temperature the FWHM remains nearly constant over about a 30 K temperature range while the FWQM shows an anomalous increase in the same temperature interval. Both the FWHM and FWQM again start to decrease and finally settle down at a temperature $T_2 = 375$, 428, 461 and 515 K for SCT12, SCT15, SCT18 and SCT21 respectively. The second transition for SCT12 ($T_2 = 375$ K) is in good agreement with the temperature at which the superlattice reflections in neutron diffraction patterns are expected to vanish due to the transition to the cubic phase (see figure 6 of part I).

The two transition temperatures ($T_1 = 475$ K and $T_2 = 510$ K) for SCT21 as obtained from the analysis of the FWHM and FWQM in figure 9 are in close agreement with the temperatures at which the unit cell constants exhibit anomalies as shown in figure 10(a) for SCT21. The cell parameters in this figure were obtained by least squares method using 220, 116, 512, 440, 532 and 228 reflections at each temperature. It is evident from this figure that the c_o parameter undergoes a small discontinuous jump around 475 K. At this temperature, the b_o parameter also shows a change of slope. At around 510 K, the a_o and b_o parameters become equal and the c_o parameter exhibits a change of slope. The elementary perovskite

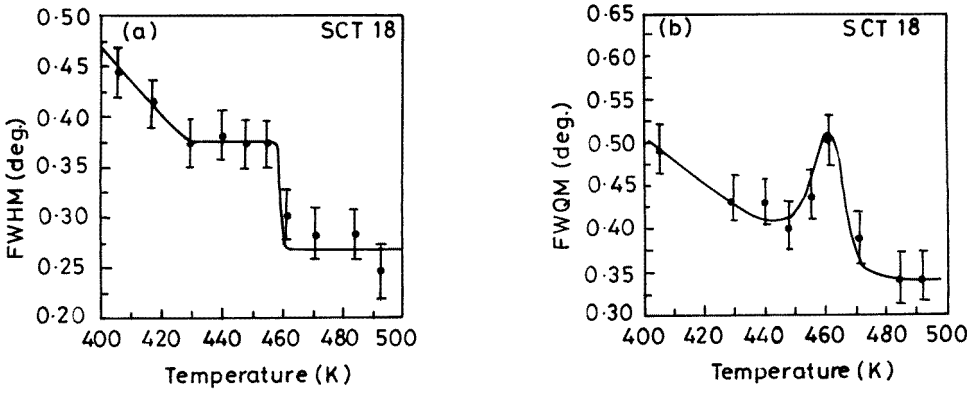

Figure 8. Temperature variation of (a) full width at half maximum (FWHM) of 228, 444, 620 triplet of reflections and (b) full width at quarter maximum (FWQM) of 008, 440 doublet for SCT18.

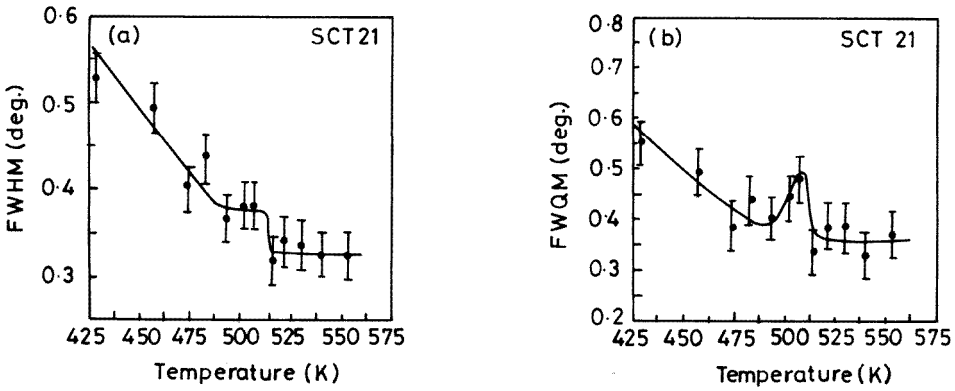

Figure 9. Temperature variation of (a) full width at half maximum (FWHM) of 228, 444, 620 triplet of reflections and (b) full width at quarter maximum (FWQM) of 008, 440 doublet for SCT21.

cell parameters derived from a_o, b_o and c_o become equal at this temperature indicating a transition to the cubic phase. The two transitions around 475 and 510 K give rise to anomalies in the unit cell volume and the coefficient of volume thermal expansion also as shown in figures 10(b) and (c) respectively. The sharp drop in the coefficient of volume thermal expansion around 475 and 510 K is due to the instabilities in the vicinity of the two transitions.

The observations presented in the preceding paragraphs suggest the existence of successive phase transitions from a room temperature orthorhombic phase to an intermediate phase at T_1 and then to the cubic phase at T_2. Redfern [7] has reported that the orthorhombic phase of pure CT also first transforms into an intermediate phase around 1423 K before becoming cubic around 1523 K. Our results indicate that the phase transition behaviour of SCT samples for $x \geqslant 0.12$ is analogous to that of pure CT. Figures 11(a), (b) depict the variation of the two transition temperatures (T_1 and T_2) with calcium content. The fact that the variation of T_1 and T_2 as a function of calcium content is quite systematic and is nearly linear from SCT12 to the CT end provides additional support to the similarity of the succession of phase transitions in SCT with $x \geqslant 0.12$ and CT. The slopes of the straight line fits in figures 11(a), (b) indicate that

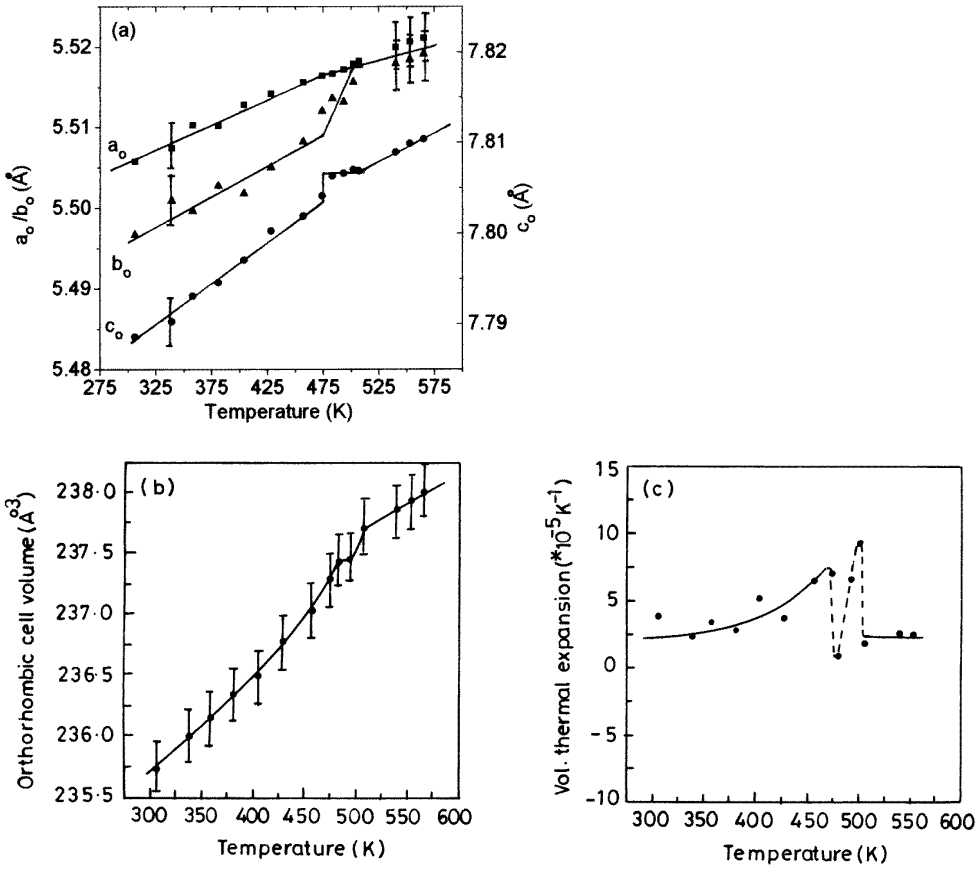

Figure 10. Temperature variation of (a) orthorhombic cell parameters, (b) unit cell volume and (c) volume thermal expansion for SCT21.

the transition temperatures T1 and T2 increase approximately at the rate of 12 and 13 K/mol% of CT in ST.

4. Concluding remarks

It is evident from the foregoing that the structure of SCT for $0.12 \leqslant x \leqslant 1.0$ is eventually cubic above a certain critical temperature. Viewed from the high temperature side, this cubic phase undergoes a succession of structural phase transitions at T_2 and T_1. With decreasing calcium content below $x = 0.12$, one expects a crossover from a CT-like structural phase transition behaviour to ST-like with only one transition temperature. As discussed in detail in part I, this crossover seems to occur somewhere in the composition range $0.06 \leqslant x < 0.12$.

The structure of SCT with $x \geqslant 0.12$ after the two transitions at T_2 and T_1 is orthorhombic belonging to the $a^-a^-c^+$ tilt system in the Glazers' classification [5, 6]. The 'antiphase' rotations (a^-a^-) about two of the pseudocubic $\langle 100 \rangle$ axes result from the condensation of the R_{25} mode. This mode in the cubic phase is triply degenerate. One would like to know whether the condensation of the two of the three of the R_{25} modes occurs simultaneously at the same temperature or in two steps. On top of this, there is condensation of the M_3 mode also which

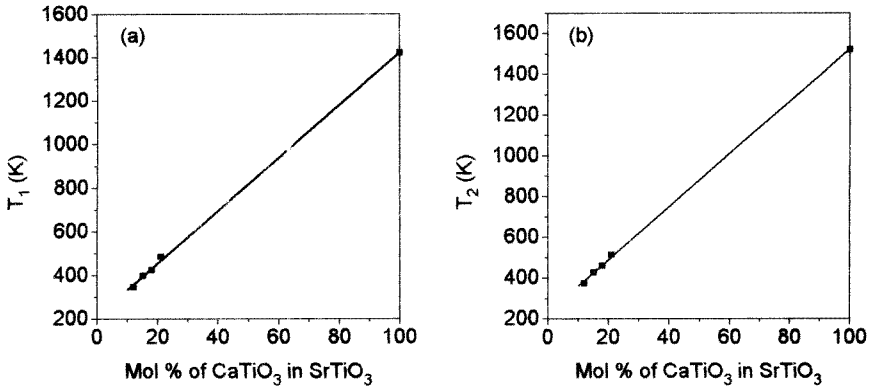

Figure 11. Variation of transition temperatures (a) T_1 and (b) T_2 of SCT with calcium concentration.

is responsible for the 'in-phase' (c^+) rotation about the third pseudocubic [100] axis. Does this M_3 mode condense independently or along with one or both of the R_{25} soft modes? This can be settled through Raman/Brillouin scattering or inelastic neutron scattering studies only which have not been carried out so far on these systems.

It is possible to infer the likely sequence of condensation of the R_{25} and M_3 modes on the basis of the critical behaviour of the intensity of the superlattice reflections. The condensation of the R_{25} leads to doubling of the pseudocubic unit cell along all the three pseudocubic $\langle 100 \rangle$ axes whereas the M_3 mode leads to doubling along only two of the three $\langle 100 \rangle$ axes. This gives rise to the so-called superlattice reflections in the elastic scattering experiments with cubic wave vectors $\boldsymbol{q}_R = 1/2(111)$ and $\boldsymbol{q}_M = 1/2(110)$. Redfern has shown that in CT the superlattice reflections with $\boldsymbol{q} = 1/2(310)$ and $\boldsymbol{q} = 1/2(113)$ disappear above 1423 and 1523 K respectively. This suggests that, viewed from the high temperature side, the first soft mode to condense corresponds to the R point of the cubic Brillouin zone followed by the freezing of the M point mode at lower transition temperature. This is similar to what is known for $KMnF_3$ with one important difference. In $KMnF_3$, the 'antiphase' rotation of the MnF_6 octahedra results from the condensation of only one of the triply degenerate R modes leading to cubic to tetragonal phase transition at 186 K. If two of the triply degenerate R modes condense simultaneously, it will lead to a cubic to orthorhombic phase transition. Structural phase transitions from cubic to tetragonal or rhombohedral phases resulting from condensation of one or all three of the R_{25} modes are known [2] to occur in materials like ST and $KMnF_3$ or $LaAlO_3$ and $PrAlO_3$. Similarly, the structural phase transition resulting from the condensation of only two of the three R_{25} modes has been reported in materials like $CsPbCl_3$ [11] which appears similar to the cubic to orthorhombic phase transition in SCT for $x \geqslant 0.12$.

Notwithstanding the possibility of the cubic to orthorhombic transition in SCT ($x \geqslant 0.12$) below T_2, it is equally probable that only one of the R_{25} modes condenses first below T_2 followed by the condensation of another R_{25} mode along with the M_3 mode. In this case, the structure of the first phase to result from the cubic phase will be tetragonal which would then transform at a still lower temperature to the orthorhombic phase of SCT/CT. Thus, there are two possible sequence of phase transitions in SCT/CT

$$\text{(i)}\ a^-a^-c^+\ (Pbnm) \xleftarrow[M_3]{T_1} a^-a^-c^0\ (Ibmm) \xleftarrow[2R_{25}]{T_2} a^0a^0a^0\ (Pm3m)$$

$$\text{(ii)}\ a^-a^-c^+\ (Pbnm) \xleftarrow[M_3,R_{25}]{T_1} a^0a^-c^0\ (I4/mcm) \xleftarrow[R_{25}]{T_2} a^0a^0a^0\ (Pm3m).$$

It is not possible to distinguish between the two possible structures for the intermediate phase on the basis of the lattice parameters since both will display a tetragonal lattice. In order to make a choice between the two possibilities, a detailed structure analysis work is required through which the correct symmetry of the atomic positions can be determined. The proposal of Redfern that the structure of the intermediate phase of the CT is tetragonal is therefore tentative pending a detailed structure analysis work. This can be checked more conveniently in SCT with higher strontium content than in pure CT because of the lower temperatures involved. We strongly recommend a simultaneous elastic and inelastic neutron scattering study of SCT for unravelling the microscopic mechanism of the structural phase transitions in this system.

Acknowledgment

We gratefully acknowledge partial support from the Inter-University Consortium for the Department of Atomic Energy Facilities (IUC-DAEF) of the Government of India. We thank one of the referees for drawing our attention to the work on $CsPbCl_3$.

References

[1] Scott J F 1974 *Rev. Mod. Phys.* **46** 83
[2] Lines M E and Glass A M 1977 *Principles and Applications of Ferroelectrics and Related Materials* (Oxford: Clarendon)
[3] Jaffe B, Cook W R and Jaffe H 1971 *Piezoelectric Ceramics* (London: Academic)
[4] Unoki H and Sakudo T 1967 *J. Phys. Soc. Japan* **23** 546
Shapiro M, Axe J D and Shirane G 1972 *Phys. Rev.* B **6** 4332
[5] Glazer A M 1972 *Acta Crystallogr.* B **28** 3384
[6] Glazer A M 1975 *Acta Crystallogr.* A **31** 756
[7] Redfern S A T 1996 *J. Phys.: Condens. Matter* **8** 8267
[8] Vogt T and Schmahl W W 1993 *Europhys. Lett.* **24** 281
[9] Mitsui T and Westphal W B 1961 *Phys. Rev.* **124** 1354
[10] Young R A, Sakthivel A, Moss T S and Paiva Santos C O 1994 *Program DBWS-9411 for Rietveld Analysis of X-ray and Neutron Powder Diffraction Pattern*
[11] Fujii Y, Hoshino S, Yamada Y and Shirane G 1974 *Phys. Rev.* B **9** 4549